*International Journal for Uncertainty Quantification*, 5 (2): 99–121 (2015)

# A NONSTATIONARY COVARIANCE FUNCTION MODEL FOR SPATIAL UNCERTAINTIES IN ELECTROSTATICALLY ACTUATED MICROSYSTEMS

*Aravind Alwan & N. R. Aluru*[*]

*Department of Mechanical Science and Engineering, Beckman Institute for Advanced Science and Technology, University of Illinois at Urbana-Champaign, 405 N. Mathews Avenue, Urbana, IL 61801, USA*

*Original Manuscript Submitted: 03/31/2014; Final Draft Received: 12/08/2014*

*This paper presents a data-driven method of estimating stochastic models that describe spatial uncertainties. Relating these uncertainties to the spatial statistics literature, we describe a general framework that can handle heterogeneous random processes by providing a parameterization for the nonstationary covariance function in terms of a transformation function and then estimating the unknown hyperparameters from data using Bayesian inference. The transformation function is specified as a displacement that transforms the coordinate space to a deformed configuration in which the covariance between points can be represented by a stationary model. This approach is then used to model spatial uncertainties in microelectromechanical actuators, where the ground plate is assumed to have a spatially varying profile. We estimate the stochastic model corresponding to the random surface using synthetic profilometric data that simulate multiple experimental measurements of ground plate surface roughness. We then demonstrate the effect of the uncertainty on the displacement of the actuator as well as on other parameters, such as the pull-in voltage. We show that the nonstationarity is essential when performing uncertainty quantification in electrostatic microactuators.*

**KEY WORDS:** *uncertainty quantification, spatial uncertainty, random process, nonstationary covariance function, Bayesian inference, microelectromechanical systems (MEMS)*

## 1. INTRODUCTION

Electrostatic actuation is the primary mechanism of generating motion in a large proportion of micromechanical transducers that are developed in the industry today. It involves generating an electric field between flexible electrodes that leads to the development of electrostatic charge on their surfaces. In the presence of electric field, this surface charge experiences a Coulombic force, which is responsible for deformation in the electrodes [1–3]. The relative magnitude of this electrostatic force scales favorably with decreasing length scales [4], making it an ideal mode of transduction in mechanical systems that are built using microfabrication technology. Although it is based on a simple and well-understood phenomenon, the design of electrostatic microactuators is a complex and challenging problem due to the numerous sources of uncertainty that must be accounted for. A major source of uncertainty is the manufacturing process itself, because the nature of microfabrication is such that it is not possible to enforce tight tolerances in physical dimensions as well as material properties. These uncertainties are frequently modeled by identifying key parameters in the device model and treating them as jointly varying random variables [5–7]. However, a more comprehensive model could include spatial variations as well in the stochastic model in order to better describe the uncertainty. In this paper, we develop a method of describing spatial nonuniformities in microelectromechanical systems (MEMS). We present a general framework for estimating stochastic models for these spatially varying parameters from profilometric data and then perform numerical simulations in order to determine the variation in output quantities of interest.

[*]Correspond to N. R. Aluru, E-mail: aluru@illinois.edu, URL: http://www.illinois.edu/∼aluru

2152–5080/15/$35.00  

Spatial nonuniformities are usually represented by random processes, which are mathematical models that describe the variation of a collection of random variables indexed by a spatial coordinate. In the context of MEMS, random processes have been used to model surface roughness that affects the measurement of electrical properties [5, 8] as well as for modeling inhomogeneous material properties, such as elastic modulus, which causes variations in thermoelastic damping of microresonators [9]. In most of these cases, the random process is assumed to have a known form and the focus is restricted to examining the influence that it plays on the physics of the device under question. However, in a realistic scenario the nature of uncertainty is usually not known and so we adopt a data-driven approach, where we estimate the stochastic process using measured data.

A typical data-driven approach involves estimating a model for the stochastic process using experimental measurements. For the case of spatially varying processes, these measurements must be made at different spatial locations in order to get an accurate idea of the spatial variation. MEMS devices are usually batch-fabricated on semiconductor or glass wafers, so that hundreds of devices can be manufactured simultaneously. Spatial variations in each processing step across the wafer can cause variations from one device to the next as well as within a single device. In this paper, we consider variations in geometrical dimensions of the device, because these are the quantities that are affected the most by spatial nonuniformities. This can be illustrated by means of the example in Fig. 1, which shows a portion of a MEMS device where a cantilever beam is suspended over a ground plate whose surface has some spatial variation. This kind of a structure is common in electrostatic actuators where a potential difference is applied between the cantilever beam and the ground plate causing an attractive force between them. This attractive electrostatic force is a function of the gap between the two electrodes and sensitive to spatial variations in these surfaces. We can model the spatial variation in the gap by repeatedly measuring the gap over a given set of devices. Data corresponding to one instance of this random variation are obtained by sampling the surface at a set of points using a profilometer, as shown in Fig. 1. This data set represents one replicate of sampled data corresponding to some unknown random process. A similar procedure can be followed for all the devices that are available, to get a set of replicates that characterize the spatial variation in the parameter of interest.

Mathematically, random processes may be characterized to the second order by the mean and covariance functions [10]. In this case, the process of estimation involves choosing the unknown parameters in the mean and covariance functions, also known as hyperparameters, using data measured at different points in domain of the random process [11]. The techniques employed in the estimation of random processes fall within the field of spatial statistics

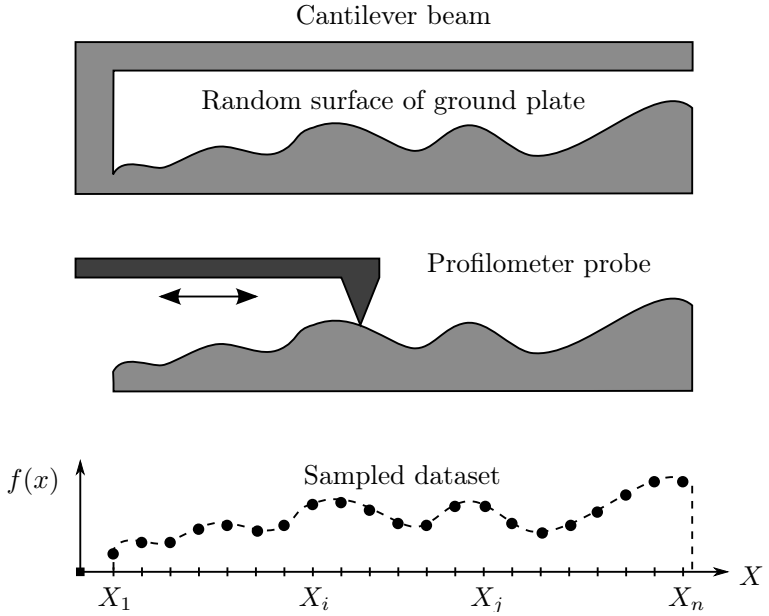


**FIG. 1:** Process of sampling surface roughness in a MEMS device.

and numerous methods have been developed for the representation of random spatially varying datasets [10, 12, 13]. While it is relatively simple to approximate the mean function by computing the average over multiple data sets, the choice of the covariance function is a more challenging task. Besag [14] developed conditional probability models that described the relation between a set of random variables associated with uniform as well as irregular lattice points in the domain. Bjørnstad and Falck [15] used continuous spline correlograms to represent the covariance function in a nonparametric manner such that it could be estimated from a given data set; whereas Zhu and Liu [16] proposed the use of a penalized likelihood estimator to learn the covariance matrix of a discrete Gauss Markov random field (GMRF) that approximates the actual random process. Other approaches include the parameter estimation of homogeneous GMRFs using a maximum likelihood approach [17] as well as the Bayesian estimation of multiscale random field models using the Markov Chain Monte Carlo (MCMC) approach [18]. In this paper, we assume that the underlying random process can be represented by a Gaussian process, which means that the joint distribution of the values at any set of points can be described by a multivariate normal distribution. Moreover, we model the covariance function using the Matérn family of covariance functions [10], because this family represents a broad class of covariance functions and is a reasonable model for a variety of physical random processes. The mean function is parametrized as a polynomial with unknown coefficients. We use the MCMC approach to learn the optimal values of the parameters that match the uncertainty in the given data.

An important aspect of modeling random processes is the assumption of stationarity, which implies that the joint probability distribution of a set of points in the domain of the random process remains the same even when the points are shifted in space. Although this assumption greatly simplifies the parametrization and estimation of random processes, it may not be valid in the general sense, especially when dealing with spatial uncertainties, such as random topography [19]. Sampson and Guttorp [20] proposed a method of estimating nonstationary spatial covariance functions through a transformation of coordinates such that the random process has a stationary covariance function in the new coordinate system. They used thin-plate splines to parametrize the transformation function and obtain the parameters by minimizing the error in the variogram of the estimated stochastic process. The question of postive definiteness of the estimated covariance function and identifiability of the nonstationary structure was formally considered in [21, 22]. This approach has also been incorporated into a Bayesian estimation framework [23]. In this work, we incorporate nonstationarity by considering a physically motivated model where we employ an additive displacement function to implement the coordinate transformation in order to model the resulting random process as stationary. We show how the physical analogy simplifies the process of imposing conditions on the displacement function and establishes a direct correspondence between these conditions and the ones derived in [21]. The entire model has been implemented in a Bayesian framework for ease of formulation and estimation.

The primary contribution in this paper is the application of data-driven stochastic models to micromechanical systems. We use the existing Gaussian process and Bayesian estimation framework to develop a procedure for estimating these models from profilometric measurements. Because nonstationarity is an inherent feature of random topography, we include this in our modeling approach to ensure that our framework can handle real data sets. We demonstrate the accuracy of our modeling approach by examining the effect of spatial uncertainties in electrostatic microactuators. Although we use synthetic data in all our examples, our goal is to put in place a generic framework that can be extended to handle actual experimentally measured data. The outline of the paper is as follows: Section 2 introduces the Bayesian estimation framework and discusses some of the relevant notation using the example of a stationary random process. The key concepts regarding the formulation of a nonstationary covariance function are developed in Section 3. This procedure is then used to estimate spatial uncertainties in a MEMS actuator and to perform UQ in the same device. Section 4 looks at the propagation of uncertainty through a multi-physics numerical model and shows the importance of including nonstationarity when simulating electromechanical devices. The concluding remarks are presented in Section 5.

## 2. MODELING SPATIALLY VARYING RANDOM FIELDS

As discussed in Section 1, we model spatially varying random fields using Gaussian processes. A Gaussian process, $f$, may be represented by a mean function, $M(X)$, which represents the expected value of the process at any point in a given domain, and a covariance function, $C(X, X')$, which describes the covariance between the values at any two

points, $X$ and $X'$, in the same domain [12]. If we consider a set of points in the domain, $\boldsymbol{X} = \{X_j; j = 1, 2, \ldots, n\}$, then the set of associated random variables, $\boldsymbol{d}$, corresponding to the values of the Gaussian process at these points, follows a multivariate Gaussian distribution as follows:

$$\boldsymbol{d} \sim \frac{1}{(2\pi)^{n/2}\,|\boldsymbol{\Sigma}|^{1/2}} \exp\left[-\frac{1}{2}(\boldsymbol{X}-\boldsymbol{\mu})^T\boldsymbol{\Sigma}^{-1}(\boldsymbol{X}-\boldsymbol{\mu})\right], \tag{1}$$

where $\boldsymbol{\mu}$ is the vector of mean values such that $\mu_j = M(X_j)$, while $\Sigma$ is the covariance matrix evaluated at the points in $\boldsymbol{X}$ and is computed as $\Sigma_{ij} = C(X_i, X_j)$, for $i, j = 1, 2, \ldots, n$ [10]. This is illustrated in Fig. 1, where we see one set of data points sampled at the points in $\boldsymbol{X}$. These values correspond to one realization of the vector of random variables, $\boldsymbol{d}$.

We first consider a simple 1D random process with a stationary covariance function to introduce some notation and to develop some concepts related to the estimation of random processes. To perform estimation, we first parametrize the random field as a Gaussian process with a polynomial mean function and a covariance function that belongs to the Matérn family of covariances as follows:

$$\begin{aligned} f|M, C &\sim GP\left(M, C\right), \\ M : X, a, b, c &\mapsto aX^2 + bX + c, \\ C : X, X', \nu, \phi, \theta &\mapsto \text{Matérn}\left(X, X', \nu, \phi, \theta\right), \\ \boldsymbol{d}|M, C &\sim \mathcal{N}\left(M(\boldsymbol{X}), C(\boldsymbol{X}, \boldsymbol{X})\right), \end{aligned} \tag{2}$$

where $\mathcal{N}\left(\boldsymbol{\mu}, \boldsymbol{\Sigma}\right)$ represents the multivariate Gaussian distribution described in Eq. (1). The Matérn covariance function is given by [10]:

$$\text{Matérn}\left(X, X', \nu, \phi, \theta\right) = \phi^2 \frac{1}{\Gamma(\nu)2^{\nu-1}} \left(\sqrt{2\nu}\frac{\|X - X'\|}{\theta}\right)^{\nu} K_{\nu}\left(\sqrt{2\nu}\frac{\|X - X'\|}{\theta}\right), \tag{3}$$

where $\Gamma$ is the Gamma function, while $K_\nu$ is the modified Bessel function of the second kind. The covariance function is parametrized by $\nu, \phi$, and $\theta$, where $\nu$ represents the differentiability of the resulting random process, while $\phi^2$ is the amplitude of the covariance function and is proportional to the pointwise variance of the random process. The term, $\theta$, is a scaling parameter that varies with the scale of the domain. We choose the Matérn covariance function because it represents a diverse class of covariances that belong to the exponential family, which is commonly used as a model to describe physical stochastic processes. When $\nu$ becomes 0, the covariance function reduces to the standard exponential covariance function, whereas the covariance function approaches a Gaussian form as $\nu$ goes to infinity. Thus, the entire random process is parametrized in terms of the unknown polynomial coefficients, $a$, $b$, and $c$, as well as the parameters of the Matérn covariance function, $\nu$, $\phi$, and $\theta$. It is important to note that this parametrization is used in this paper only for illustration and a more general form may be used in a practical situation. For instance, the mean function could be represented in terms of a sinusoidal basis, while a different kernel function could be used as the covariance function. The choice of this parametrization is left to the user depending on the properties of the data that is available.

The process of estimating the random process involves choosing an appropriate set of values for the unknown parameters in Eq. (2) for a given set of values for $\boldsymbol{d}$, so that the resulting random process closely matches the actual, unknown process from which the data set is derived. Instead of obtaining point estimates for these parameters, we use Bayesian inference where the goal is to estimate the associated probability density function (PDF) for each of them. We assign a prior PDF for each parameter based on any known information that we may have and then use Bayes theorem to derive the posterior PDF based on the prior PDF and the likelihood of observing the given data set. Finally, we draw samples from the posterior PDF using the Metropolis-Hastings algorithm to obtain realizations of the stochastic process that are consistent with the given data [24]. This process is known as the Markov Chain Monte Carlo method, and in this paper, we implement this algorithm using the popular Python software library, PyMC [25]. We illustrate the steps involved by means of an example that is described below.

In this paper, we do not use actual experimental data for estimating the stochastic processes. Instead we demonstrate a proof of concept by generating data that vary according to a known distribution. This allows us to check the veracity of estimated models by comparing to the actual one. Consider a 1D random process that is described by a mean function and a covariance function. We generate realizations of this random process and sample these realizations at uniformly spaced points. After sampling the data, we set aside the actual random process and proceed to estimate the stochastic process using only the data and some prior assumptions that we make regarding the form of the random process. In other words, the sampled data are used as the input for estimation, where we try to reconstruct the parameters of the actual stochastic process from which the data originated. To generate the data, we use a stochastic process that is defined in the $[0, 1]$ domain with a linear mean function given by $M(X) = 0.1X$ and a stationary, isotropic Matérn covariance function given by Eq. (3) with the parameters: $\phi = 0.02$, $\nu = 2$, and $\theta = 0.2$. Figure 2 shows some realizations that have been sampled from this stochastic process and a contour plot of the corresponding covariance function.

We sample the realizations generated from the actual stochastic process at a set of 41 uniformly spaced points $\boldsymbol{X}$ to create a set of values for $\boldsymbol{d}$, which simulates profilometric data that are aggregated over many different realizations. We ensure that the number of samples is large enough so that the statistical properties of the data match the actual mean and covariance function quite closely, i.e., $\mathbb{E}[d_j] \sim M(X_j)$ and $Var[d_i, d_j] \sim C(X_i, X_j) \forall i, j = 1, 2, \ldots, n$. Because the standard Matérn covariance function is a symmetric stationary covariance function, the covariance between the values of the random process at any two points depends only on the distance between the points and is independent of the locations of the points themselves. This is seen from Eq. (3), where the covariance between the values at $X$ and $X'$ depends only on $\|X - X'\|$. This can also be independently verified by computing the correlation between every pair of values in $\boldsymbol{d}$. Figure 3 plots the normalized covariance between every pair of values as a function of the distance between their physical locations. We see that the points coincide quite well with the solid line, which corresponds to the actual covariance function, showing that the process is indeed stationary.

Using the data sampled over 250 realizations, we perform Bayesian estimation to obtain estimates for the unknown parameters in Eq. (2). The first step involves choosing the prior PDFs for these parameters. In the absence of any definite prior information, we choose vague priors with arbitrary values for most of the parameters. Because some of the quantities like $\nu$, $\phi$, and $\theta$ must be positive for the Matérn covariance function to be well-defined, we choose appropriate prior PDFs that are nonzero only for positive values. We note that the parameter $\nu$ determines the differentiability of the sample paths of the stochastic process and must have a value of $>1$ in order for the paths to be differentiable. In the following sections, we shall examine in greater detail the requirement that the realizations

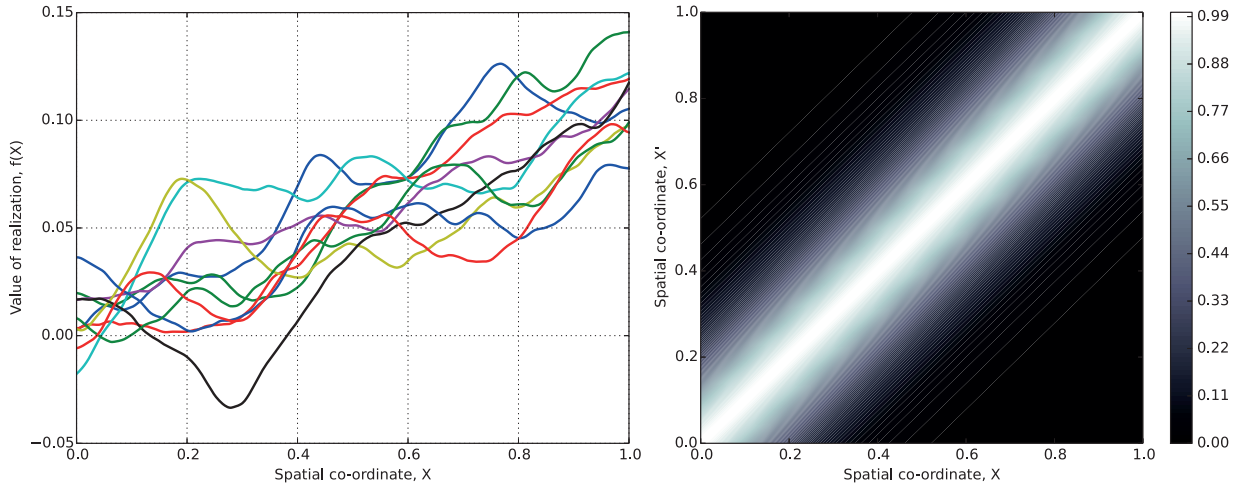


(a) Realizations of the actual stochastic process (b) Covariance function

**FIG. 2:** Actual stochastic process described in Section 2 illustrated by (a) sampled realizations and (b) contour plot of the covariance between points in the domain.

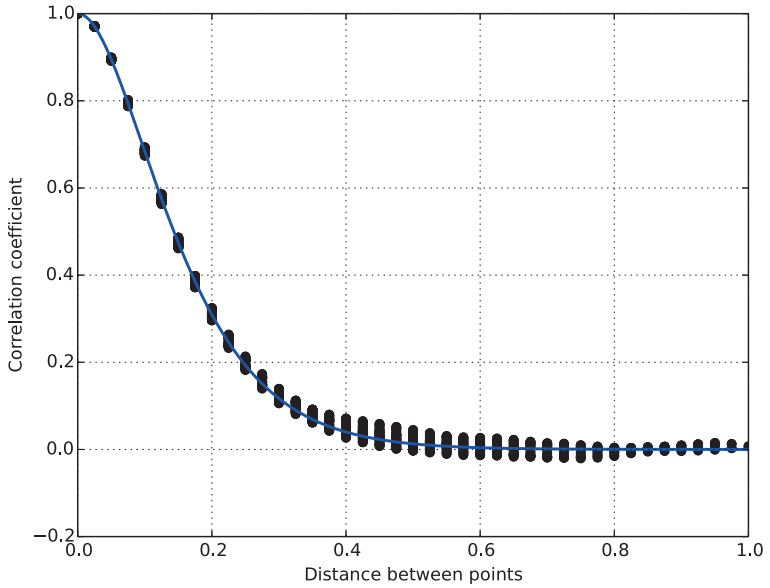


**FIG. 3:** Normalized covariance between sampling points as a function of the distance between them. The solid line represents the actual Matérn covariance function.

be differentiable. For the moment, we shall assume this condition and incorporate it into the prior PDFs as well. If some definite information is available regarding the distribution corresponding to the unknown parameters, it can be incorporated into the prior PDFs in a suitable form (e.g., we have chosen an exponential distribution for $\phi$ and $\theta$ since we know that these parameters must always be positive). Similarly, we have chosen a suitable range for $\nu$ so that the resulting random process is differentiable. Apart from these restrictions, we choose the prior PDFs to be quite general, so that the estimation process is not skewed as a result of a choice of priors. In our numerical tests, we have repeatedly performed the estimation using different randomly chosen values for the prior PDF parameters and have not observed any significant variation in the results. The final set of prior PDFs are as follows:

$$\begin{aligned} a, b, c &\sim \text{Uniform}[-1, 1], \\ \nu &\sim \text{Uniform}[1, 3], \\ \phi &\sim \text{Exponential}(10), \\ \theta &\sim \text{Exponential}(1). \end{aligned} \tag{4}$$

Finally, we use the MCMC method to derive posterior PDFs for all the unknown parameters and sample from their joint density to obtain estimates for each of them. This involves using the Metropolis-Hastings algorithm to generate a sequence of samples that are drawn from the posterior PDF. We applied a process of "burn-in," where we discarded the first 30,000 iterations and thinned the remaining by a factor of 10 to finally obtain a set of 1000 samples for each parameter. Burn-in is used to minimize the dependence of the samples on the initial values, while thinning ensures that the samples are not correlated with one another so that the resulting set may be assumed to be independently drawn.

We plot histograms of the unknown parameters and compare their statistical measures to the corresponding expected values. Figure 4(a) contains histogram plots of $a$, $b$, and $c$ in the mean function, whereas Fig. 4(b) shows similar statistics for the parameters, $\nu$, $\phi$ and $\theta$ in the covariance function. We also compare the mean values for the estimated parameters with the actual values used in the original stochastic process in Table 1 and see that the estimated values are accurate. Table 1 also shows the sampling error in the estimates, which is computed as the standard deviation over the averages computed for 100 random subsets of the values. In most of the cases, the magnitude of sampling error is quite small compared to the mean, which shows that the estimates are trustworthy.

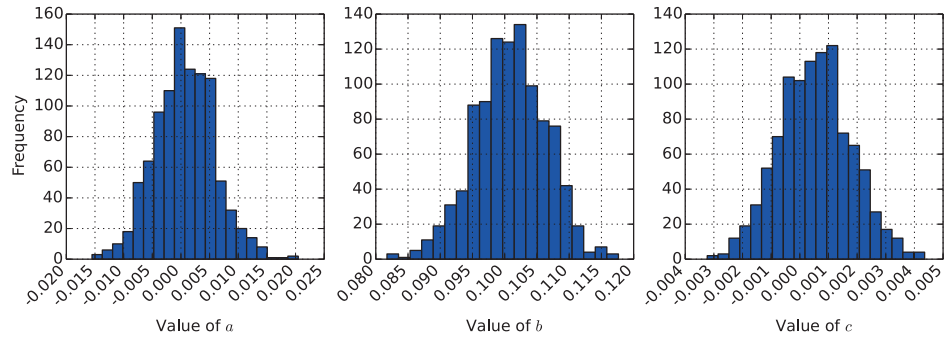


(a) Histograms of $a$, $b$, and $c$, respectively

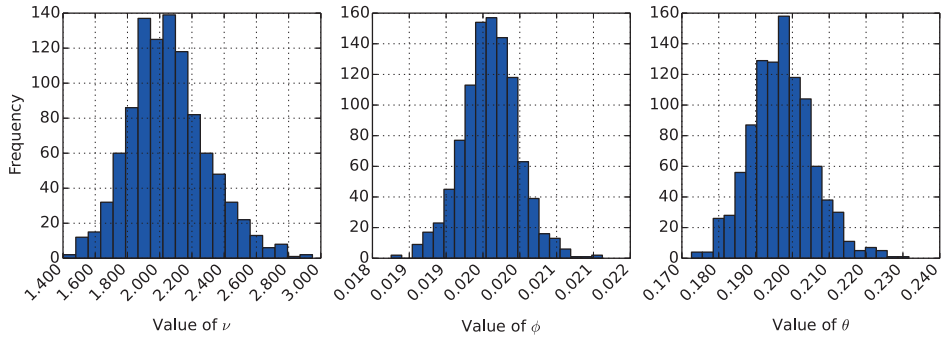


(b) Histograms of ν, ϕ, and θ, respectively

**FIG. 4:** Histograms of the estimated parameters in the (a) mean function and (b) covariance function for the example described in Section 2.

**TABLE 1:** Estimated parameter means compared with actual values for test case in Section 2

| Parameter | Actual value | Estimated mean value |
|---|---|---|
| $a$ | 0 | $0.0006 \pm 0.0005$ |
| $b$ | 0.1 | $0.1009 \pm 0.0005$ |
| $c$ | 0 | $(5.3 \pm 0.9) \times 10^{-4}$ |
| ν | 2 | $2.05 \pm 0.002$ |
| ϕ | 0.02 | $0.02010 \pm 0.00002$ |
| θ | 0.2 | $0.1971 \pm 0.0006$ |
| B | n.a. | 1.994 |

Although comparing the mean values of the estimated parameters under their respective posterior distributions is a reasonable way of verifying that the estimation procedure is correct, it is not a comprehensive test because it only compares the average values. A more rigorous method of verifying the estimated model involves computing the Bayes factor. It has been extensively used in model selection problems where the goal is to choose an appropriate model between two or more possible options [26]. The Bayes factor, $B$, is defined as the ratio of the likelihood of the data conditioned on the estimated model to the likelihood conditioned on the actual model as follows:

$$B = \frac{\Pr\left(\boldsymbol{d}|P_{\text{estimated}}\right)}{\Pr\left(\boldsymbol{d}|P_{\text{actual}}\right)} = \underbrace{\frac{\Pr\left(P_{\text{estimated}}|\boldsymbol{d}\right)}{\Pr\left(P_{\text{actual}}|\boldsymbol{d}\right)}}_{\text{Posterior odds}} \Bigg/ \underbrace{\frac{\Pr\left(P_{\text{estimated}}\right)}{\Pr\left(P_{\text{actual}}\right)}}_{\text{Prior odds}}, \tag{5}$$

where $P_{\text{actual}}$ and $P_{\text{estimated}}$ represent the actual and estimated models, respectively. Unlike point estimates of model parameters, the Bayes factor uses the likelihoods marginalized over the set of model parameters. Equation (5) also shows that the Bayes factor may be expressed as a ratio of the posterior odds between the two models to the prior odds between them. This form removes the need to integrate over all the model parameters in order to calculate the marginal likelihoods and can be easily computed during the MCMC process. The Bayes factor for the estimated model is given in Table 1. On the basis of the scale given by Jeffreys [27], if the Bayes factor is $<3$, then the difference between the estimated and the actual models is barely worth mentioning.

The advantage of using a Gaussian process-based framework is that although the given data is a discrete sample that is obtained over a finite set of locations, by estimating the mean and covariance functions, we get a continuous representation for the estimated random process. Figure 5 shows some realizations of the estimated stochastic process for this example. This allows us to draw realizations of the estimated process, which can then be used to perform UQ.

## 3. NONSTATIONARY COVARIANCE FUNCTIONS

In order to generalize the above formulation to handle nonstationary covariance functions, we establish a mapping between the actual covariance function and an equivalent stationary covariance function that is obtained by means of a coordinate transformation [20]. For a point located at $X$, we apply a displacement, $u(X)$, to move it to a new position, $x$, which we denote as the displaced position. The displacement function, $u(X)$, is initially unknown, and we want to choose it such that $C(x, x')$ is a stationary covariance function. We shall continue to use the Matérn family to model this covariance function. This gives us the following nonstationary formulation for the random process:

$$\begin{aligned} f|M, C &\sim GP\left(M, C\right), \\ M : X, a, b, c &\mapsto aX^2 + bX + c, \\ C : x, x', \nu, \phi, \theta &\mapsto \text{Matérn}\left(x, x', \nu, \phi, \theta\right), \\ x : X, u &\mapsto X + u(X) \\ u : X, a_u, b_u, c_u, d_u &\mapsto a_u X^3 + b_u X^2 + c_u X + d_u, \\ \boldsymbol{d}|M, C &\sim \mathcal{N}\left(M(\boldsymbol{X}), C(x(\boldsymbol{X}), x(\boldsymbol{X}))\right), \end{aligned} \tag{6}$$

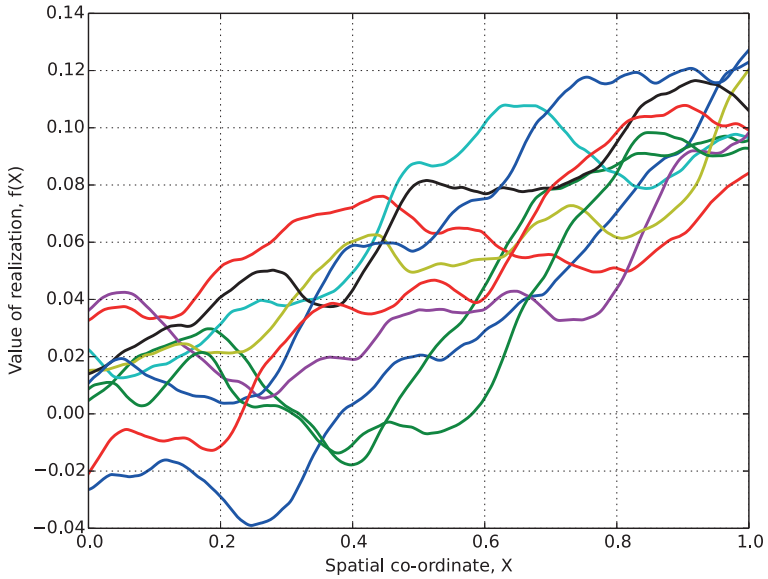


**FIG. 5:** Realizations of the estimated stochastic process described in Section 2.

where we have parametrized $u(X)$ as a cubic polynomial. Equation (6) is identical to the formulation presented in Section 2 except for the addition of four extra parameters that describe the variation of the displacement field. The choice of parametrization used for $u(x)$ is left to the discretion of the user. In this paper, we have chosen a polynomial basis as the simplest representation of the displacement function. This representation works well as long as the actual displacement function can be represented by a finite polynomial series. This can be empirically shown to be true, by choosing the order of the polynomial to be sufficiently high. We observe that the mean value of the posterior PDF for each of the coefficients of higher order terms tends to zero, showing that the displacement function does not depend on those terms. In practice, if this condition is not met, then it may be appropriate to use a different basis for the representation. Alternatively, one could use a different representation using thin-plate splines or some other basis with local support as shown in [20]. To estimate the parameters from data sets, we make use of the same Bayesian inference procedure developed in Section 2.

As in Section 2, we choose an illustrative example to demonstrate the method. We generate data from a known random process that is defined in the domain $[-1, 1]$ with a quadratic mean function, $M(X) = 10X^2 + 5$, and a Matérn covariance function with the parameters $\phi = 2$, $\nu = 2$, and $\theta = 0.4$. Nonstationarity is introduced using the displacement function, and we choose two cases to demonstrate two different forms of nonstationarity. We denote $u(X) = 0.5X(1 - X^2)$ as Case I. This corresponds to a displacement that is directed outward from the origin. Case II is the opposite with $u(X) = -0.5X(1 - X^2)$, which corresponds to a displacement that is directed toward the origin. In both cases, the form of the displacement function has been chosen such that it is zero at $X = 0$ as well as at both the left and right boundaries of the domain.

Figure 6 shows sample realizations and a contour plot of the covariance function for Case I. We see a distinct difference in the smoothness of the sample paths between the center and the edges. It is easy to visualize that because the displacement function is positive at points lying on either side of 0 and the region in the center is under tension whereas the edges are in compression. As a result, the distance between points is increased in the center region, causing the covariance function to drop down to zero more quickly. This decreases the amount of correlation between the values at neighboring points and is reflected in the sample paths as an increased roughness in the center. In comparison, compression in the boundary regions causes points to come closer and hence increase the correlation between them, leading to smoother curves. We see the exact reverse of this situation in Case II (shown in Fig. 7), where the center is relatively smooth while the edges are rougher.

The nonstationarity of the covariance function can also be illustrated by plotting the normalized covariance between points in the data set. Figure 8 shows the plots for both Cases I and II. Comparing them to Fig. 3, we see that

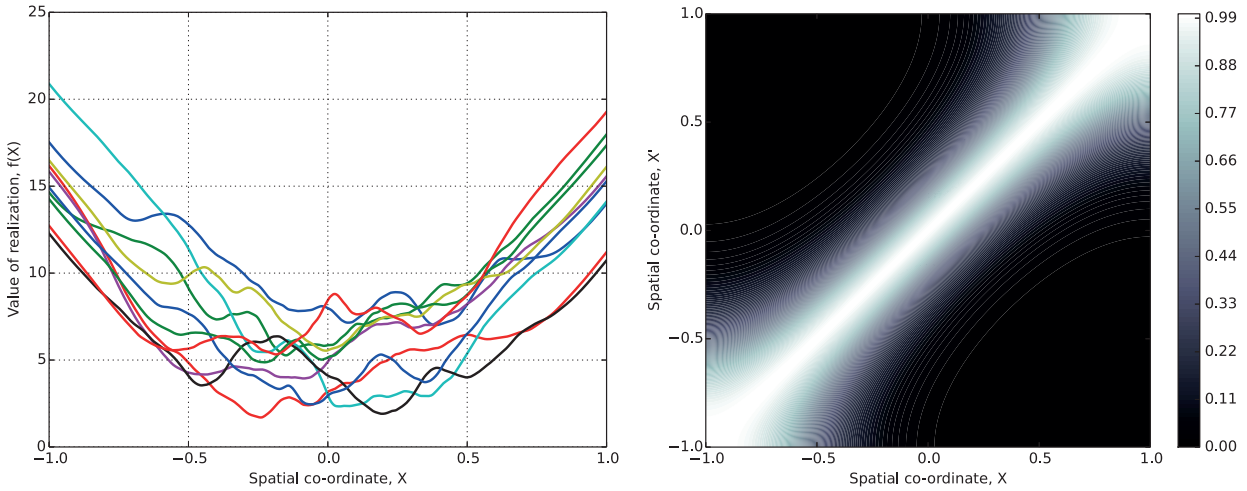


(a) Realizations of the actual stochastic process (b) Covariance function

**FIG. 6:** Actual nonstationary stochastic process corresponding to Case I illustrated by (a) sampled realizations and (b) contour plot of the covariance between points in the domain.

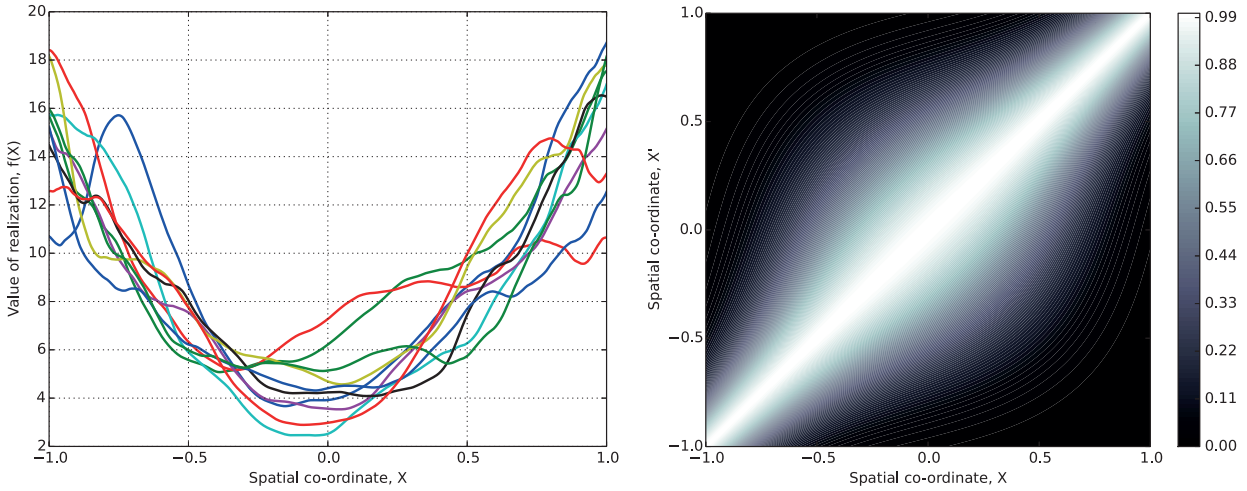


(a) Realizations of the actual stochastic process (b) Covariance function

**FIG. 7:** Actual nonstationary stochastic process corresponding to Case II illustrated by (a) sampled realizations and (b) contour plot of the covariance between points in the domain.

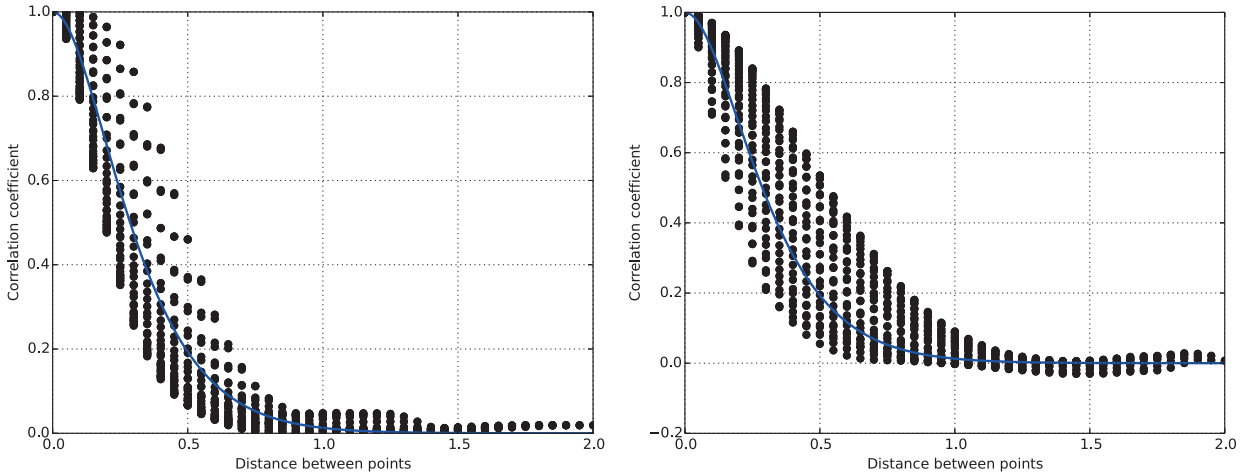


(a) Case I (b) Case II

**FIG. 8:** Normalized covariance between sampling points as a function of the distance between them. The solid line represents the stationary Matérn covariance function.

the points deviate significantly from the solid line that represents the stationary covariance function, showing that the data are derived from a process that is indeed nonstationary.

### 3.1 Uniqueness and Identifiability of the Displacement Function

Before we look at the estimation of the random process, we first consider the issues related to uniqueness and identifiability of the displacement function. Although $u(X)$ may be represented using any functional form, it is important to ensure that even after the coordinate transformation, $C(x, x')$ continues to be a valid covariance function. Moreover, we want to choose a parametrization for $u(X)$ such that it can be uniquely determined from the given data. In this section, we place additional constraints on $u(X)$ so that these conditions are satisfied.

The question of validity of the nonstationary covariance function is easy to tackle. We must ensure that even after the coordinate transformation, the covariance function retains its properties of being symmetric and positive-definite. Because our formulation based on the Matérn covariance function ensures that $C(x, x') = C(|x - x'|)$, we can readily see that it is symmetric. The positive-definiteness property of this form also remains unaffected as a result of this transformation, and this can be easily proved by applying Bochner's theorem [12].

In addition to the validity, we are also interested in the identifiability of the displacement function and in turn, the covariance function. In order to ensure that the parameters of the displacement function can be uniquely determined from the given data, we want to enforce a bijective mapping between the parameters and the resulting covariance function. Unfortunately due to the presence of norm operator in the covariance function, particular cases of the displacement function can cause the mapping to cease being unique. More precisely, this situation arises whenever the left-to-right ordering of two points in the domain gets reversed in the deformed coordinate system as a result of any relative displacement that causes them to cross each other. We can see that the limiting case that corresponds to the onset of this problem occurs when the displacement causes two distinct points in $X$ to get mapped on to the same point in $x$.

In order to ensure a bijective mapping, we want to restrict the possible values of the displacement function so that no two points cross each other in the deformed space. Physically, this condition implies that the strain field that corresponds to the displacement does not cause gaps or overlaps in the body. This compatiblity condition can be reduced to the assertion that the determinant of the Jacobian of transformation is always positive. In one dimension, this determinant is nothing but $1+du/dX$, and thus we derive the condition that in order for the displacement function to be uniquely determined, we must ensure that

$$\frac{du(X)}{dX} > -1. \tag{7}$$

We can also prove the validity of this condition mathematically. Perrin and Meiring [21] derive a uniqueness condition for a general transformation function and express this condition in terms of the inverse of the Jacobian of transformation. We can immediately see that in order for this condition to be well defined, the Jacobian must be nonsingular and hence, its determinant must be nonzero. Thus we get the same condition as that expressed in Eq. (7). This condition can be easily incorporated into our estimation framework given by Eq. (6), by constraining the parameters that govern the displacement function. We impose the additional condition, that

$$3a_u X^2 + 2b_u X + c_u > -1 \quad \forall X \in \mathcal{D}, \tag{8}$$

where $\mathcal{D}$ is the domain in which the stochastic process is defined. This condition is applied when drawing samples for the posterior PDF to ensure that the resulting displacement function satisfies the uniqueness condition. We see the benefit of choosing the parametric formulation given in Eq. (6) involving an additive displacement function, in that it allows for the incorporation of the uniqueness condition while retaining a physical intuition for the estimation framework.

There is one final observation that we can make regarding the displacement function. We can show that the addition of any linear term to the displacement function does not affect the value of the covariance function as long as $\theta$ is scaled by an appropriate constant. In other words, the displacement function is uniquely determinable only to a linear function and $\theta$ to within a constant factor. We can show this for our specific parametrization by considering the following transformation to the argument of the covariance function

$$\begin{aligned}
&\frac{\|x(X) - x'(X')\|}{\theta} = \frac{\|X + u(X) - X' - u(X')\|}{\theta} = \frac{\|(X - X') + a_u(X^3 - X'^3) + b_u(X^2 - X'^2) + c_u(X - X')\|}{\theta} \\
&= \frac{\|(X - X') + a_u(X^3 - X'^3) + b_u(X^2 - X'^2) - (a_u + b_u)(X - X') + (a_u + b_u + c_u)(X - X')\|}{\theta} \\
&= \frac{\|(1 + a_u + b_u + c_u)(X - X') + a_u(X^3 - X'^3) + b_u(X^2 - X'^2) - (a_u + b_u)(X - X')\|}{\theta} \\
&= \frac{\|(X - X') + a_u^*(X^3 - X'^3) + b_u^*(X^2 - X'^2) - (a_u^* + b_u^*)(X - X')\|}{\theta^*},
\end{aligned} \tag{9}$$

where $k^* = k/(1+a_u+b_u+c_u)$ for each of the terms, $a_u^*$, $b_u^*$, and $\theta^*$. We see that the value of the covariance function does not change when the parametrization of $u(X)$ is modified by the addition or subtraction of a linear term. This property is borne out in [21] where the authors qualify the uniqueness criterion by stating that the transformation is unique only up to a scaling factor for $\theta$ and a homothetic Euclidean motion for the transformation function. We can therefore use a corrected form of $u(x)$ given by

$$u : X, a_u^*, b_u^* \mapsto a_u^* X^3 + b_u^* X^2 - (a_u^* + b_u^*)X. \tag{10}$$

In the discussion below, we talk about this corrected form of $u(X)$ in addition to the original form since this form has the property that the displacement is zero at the two boundaries of the domain. This makes it easy to compare the corrected form with the actual displacement function, since this is a property shared by the actual function as well. It must be noted that the estimated covariance function remains the same in either case and hence, the properties of the estimated random process do not change.

### 3.2 Estimation of Nonstationary Random Processes

Using the data sets generated for Cases I and II presented earlier, we estimate the corresponding stochastic processes. We employ the formulation given in Eq. (6) and assign the following prior PDFs for the unknown parameters:

$$\begin{aligned} a, b, c &\sim \text{Uniform}\,[-20, 20], \\ \nu &\sim \text{Uniform}\,[1, 3], \\ \phi &\sim \text{Exponential}\,(1) \\ \theta, \theta^* &\sim \text{Exponential}\,(1) \\ a_u, b_u, c_u, d_u, a_u^*, b_u^* &\sim \text{Uniform}\,[-1, 1]. \end{aligned} \tag{11}$$

As in the case of stationary covariance functions presented in Section 2, the prior PDFs can be specifically chosen to incorporate any knowledge we may have on the values of the unknown parameters or can be left sufficiently vague in the absence of such information. We note that in addition to the usual parameters that control the mean and covariance functions, we now have an additional set of parameters that describe the displacement function used to incorporate nonstationarity. Using data sampled over 250 randomly generated realizations at 41 equally spaced points, we generate the joint posterior distribution of the parameters and pick 1000 samples from it by using the MCMC method with a burn-in of 30,000 and a thinning factor of 10.

The estimated mean value of each of the unknown parameters is compared with their actual values for both Cases I and II in Table 2. For both cases, we see a very good match between the actual and estimated values for all parameters that directly affect the mean and covariance function. There is some error in the estimated values of $a$ and $b$ for Case II, which is possibly due to statistical error in the data samples. However, for the polynomial coefficients that govern the displacement function, $a_u$, $b_u$, and $c_u$, we see that there is a large mismatch between the estimated and actual values. This discrepancy is to be expected because the displacement function and, by extension its polynomial coefficients, can be determined uniquely only up to a linear term. To confirm that the covariance function has indeed been estimated properly, we examine the parameters corresponding to the corrected form of the displacement function, namely, $a_u^*$, $b_u^*$, and $\theta^*$. We compute these parameters using the expressions derived in Eq. (9). By construction, the corrected form of the displacement function has been specifically chosen to match the actual function at the boundaries of the domain and, therefore, we see a very good match between the estimated values of these parameters and the actual ones. This is further attested to by the comparison of the estimated displacement function to the actual one in Fig. 9, where we see an almost perfect match between the corrected form and the actual function. Because we have shown that the two forms of the displacement function ultimately yield the same value of covariance, we are free to use either form when generating realizations that conform to the estimated random process.

Using the parameters estimated from the sampled data, we can now construct realizations of the random process. A few sample realizations are shown for Cases I and II in Fig. 10. Comparing to samples shown in Figs. 6(a) and

**TABLE 2:** Estimated parameter means compared to actual values for test cases in Section 3.2

| | Case I | | Case II | |
|---|---|---|---|---|
| Parameter | Actual value | Estimated mean value | Actual value | Estimated mean value |
| a | 10 | $10.0036 \pm 0.0001$ | 10 | $9.933 \pm 0.007$ |
| b | 0 | $-0.0135 \pm 0.0002$ | 0 | $0.063 \pm 0.002$ |
| c | 5 | $4.951 \pm 0.002$ | 5 | $5.208 \pm 0.005$ |
| $\nu$ | 2 | $2.0047 \pm 0.0009$ | 2 | $2.029 \pm 0.001$ |
| $\phi$ | 2 | $1.979 \pm 0.002$ | 2 | $1.959 \pm 0.002$ |
| $\theta$ | 0.4 | $0.3808 \pm 0.0005$ | 0.4 | $0.572 \pm 0.008$ |
| $a_u$ | –0.5 | $-0.4788 \pm 0.0003$ | 0.5 | $0.737 \pm 0.01$ |
| $b_u$ | 0 | $-(2.77 \pm 0.08) \times 10^{-4}$ | 0 | $0.006 \pm 0.0002$ |
| $c_u$ | 0.5 | $-0.437 \pm 0.001$ | –0.5 | $-0.258 \pm 0.01$ |
| $d_u$ | 0 | $-0.02 \pm 0.02$ | 0 | $-0.009 \pm 0.02$ |
| $a_u^*$ | –0.5 | –0.4998 | 0.5 | 0.496 |
| $b_u^*$ | 0 | –0.0001 | 0 | 0.004 |
| $\theta^*$ | 0.4 | 0.3975 | 0.4 | 0.385 |
| B | n.a. | 1.343 | n.a. | 1.736 |

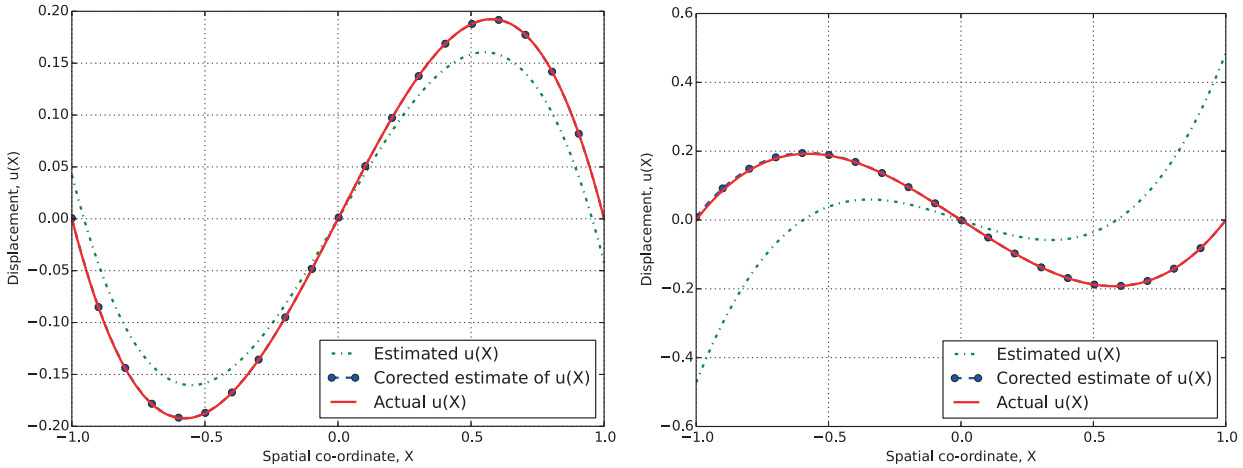


(a) Case I (b) Case II

**FIG. 9:** Estimated displacement functions for (a) Case I and (b) Case II. Solid lines show the actual displacement function, dash-dotted lines represent the estimated displacement using the original formulation and dashed lines represent the estimated function using the corrected formulation.

7(a), we see a qualitative match between the two. The estimated realizations clearly capture the nonstationarity in the random process, proving that this method is suitable for estimating spatially varying uncertainties with nonstationary covariance functions.

## 4. APPLICATION TO MICROACTUATORS

We now use the random process estimation framework described above to generate stochastic models for spatial uncertainties in a micromechanical actuator. We first discuss the physical modeling of the actuator, followed by examples that demonstrate the effect of spatial variations on the actuator behavior.

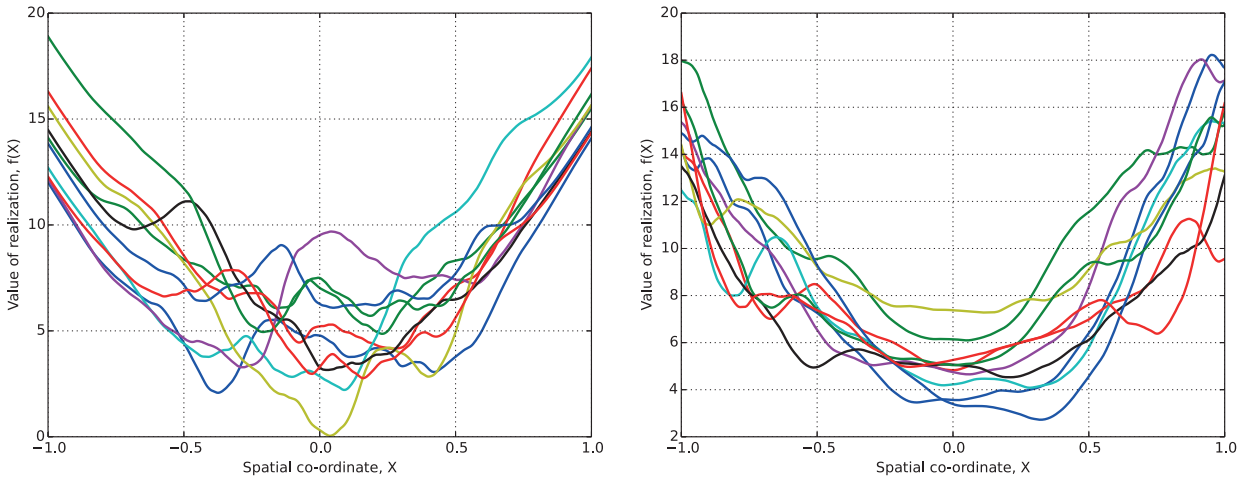


(a) Case I (b) Case II

**FIG. 10:** Realizations sampled from estimated stochastic process for (a) Case I and (b) Case II.

### 4.1 Physical Level Modeling

We are primarily interested in performing UQ for microelectromechanical actuators, which employ electrostatic force as the primary actuation mechanism. These actuators are typically modeled as a pair of electrodes, of which one is deformable while the other is held fixed at a small distance away. The region between the electrodes is considered to be a uniform dielectric material, usually air. A potential difference that is applied across the two electrodes sets up an electric field in the region between them. This results in an attractive electrostatic force on the compliant electrode, causing it to deform. Because the electric field, and hence the electrostatic force, is a function of the separation between the electrodes, we solve for the electrostatic potential in the dielectric and the actuator displacement in a coupled manner to ensure a consistent solution. We can thus obtain the steady-state displacement of the actuator as a function of the applied voltage.

We model the actuator domain as shown in Fig. 11. The two electrodes are assumed to be perfect conductors and are represented in their initial undeformed configuration as $\Omega_1$ and $\Omega_2$, respectively, while $\overline{\Omega}$ refers to the dielectric region surrounding the electrodes. The top electrode is deformable and anchored at the left end. We seek the

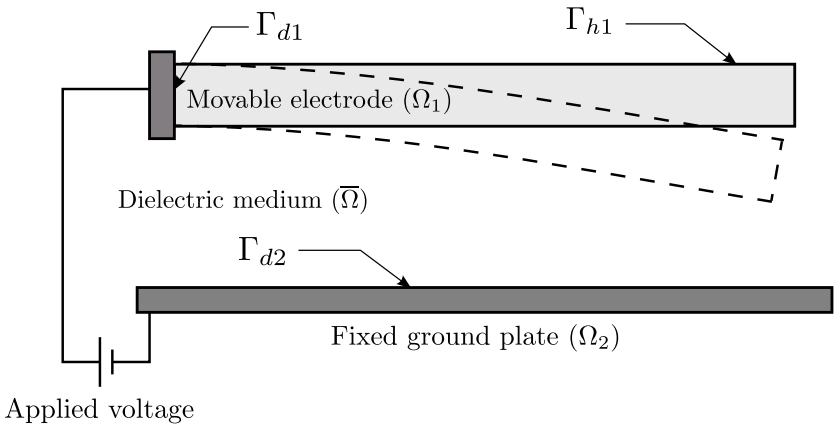


**FIG. 11:** Electrostatic microactuator (not drawn to scale) consisting of a cantilever beam that deforms under the influence of electrostatic force that is produced due to the applied potential difference.

equilibrium solution of the coupled equations for the electrostatic potential and the mechanical displacement in the deformed configuration that is attained when a constant potential difference is applied. This is done by expressing the equations using a Lagrangian formulation, where the equations are mapped back to the undeformed configuration by means of the deformation gradient, $\boldsymbol{F}$. Using a 2D geometrically nonlinear formulation [28], the displacement of the deformable electrode is given by

$$\nabla \cdot (\boldsymbol{F}\boldsymbol{S}) = 0 \text{ in } \Omega_1, \tag{12}$$

$$\boldsymbol{u} = 0 \text{ on } \Gamma_{d1}, \Gamma_{d2}, \tag{13}$$

$$\boldsymbol{P}\boldsymbol{N} = \boldsymbol{H} \text{ on } \Gamma_{h1}, \tag{14}$$

where $\boldsymbol{u}$ is the vector field denoting the displacement, $\boldsymbol{F} = \boldsymbol{I} + \nabla \boldsymbol{u}$, $\boldsymbol{I}$ being the identity tensor, $\Gamma_{d1}$ and $\Gamma_{d2}$ are the anchored portions of the electrode boundaries where a Dirichlet boundary condition is applied, $\boldsymbol{P}$ is the first Piola-Kirchhoff stress tensor, $\boldsymbol{N}$ is the outward normal vector at every part of the boundary in the reference configuration, and $\boldsymbol{H}$ is the boundary traction vector that corresponds to the electrostatic traction acting on the free surfaces of the movable electrode, $\Gamma_{h1}$. $\boldsymbol{S}$ in Eq. (12) is the second Piola-Kirchhoff stress tensor that can be expressed in terms of a constitutive relationship involving the material tensor, $\boldsymbol{C}$, and Green-Lagrangian strain tensor, $\boldsymbol{E_s}$, as [29],

$$\boldsymbol{S} = \boldsymbol{C}\boldsymbol{E_s}. \tag{15}$$

We see that the driving force for the mechanical displacement is the electrostatic traction, which can be obtained by solving for the electrostatic potential. Because the electrodes are assumed to be metallic, the electric field within them is zero and thus, it is sufficient to solve for the potential field in the dielectric region surrounding the electrodes. This can be written in terms of the Laplace equation, with a Dirichlet boundary condition on the boundaries of the electrodes, as follows:

$$\nabla \cdot \left(J\boldsymbol{F}^{-1}\boldsymbol{F}^{-T}\nabla\phi\right) = 0 \text{ in } \overline{\Omega}, \tag{16}$$

$$\phi = \phi_0 \text{ on } \Gamma_{d1}, \Gamma_{d2}, \Gamma_{h1} \tag{17}$$

where $J = \det\boldsymbol{F}$ is the Jacobian of the deformation gradient and $\phi_0$ is the prescribed potential applied on the boundaries of the electrodes. The electrostatic potential that is obtained by solving Eq. (16) is coupled back to the mechanical displacement by way of the electrostatic traction term, $\boldsymbol{H}$, which is given by

$$\boldsymbol{H} = J\left|\boldsymbol{F}^{-T}\boldsymbol{N}\right|\boldsymbol{f}_{es}, \tag{18}$$

where $\boldsymbol{f}_{es}$ is the electrostatic traction acting on the movable electrode in the deformed configuration. This traction depends on the normal electric field at the interface between the electrode and the dielectric, $E_n$, and the surface charge density, $\sigma_s = \epsilon E_n$, where $E_n$ is the normal component of the electric field, $\boldsymbol{E} = -\nabla\phi$, along the unit normal vector, $n$, in the deformed configuration. The complete expression for the electrostatic traction is given by $\boldsymbol{f}_{es} = [{\sigma_s}^2/(2\epsilon)]\boldsymbol{n}$, where $\epsilon$ is the dielectric permittivity of the surrounding medium.

In practice, we do not solve Eq. (16) directly, because it is defined over $\overline{\Omega}$, which is infinitely large. Instead we transform this equation using boundary integral formulation [30, 31] into a set of integral equations defined on the boundaries of the electrodes. The boundary integral formulation is an efficient way of solving the Laplace equation for exterior-domain problems such as this one. Additional details about this procedure are given in [3, 32].

The electrostatic microactuator chosen in this example consists of a cantilever beam that is 100 μm long, 1μm thick and made of silicon with a Young's modulus of 169 GPa. It is held at a distance of 2 μm from the ground plate, which is assumed to extend an additional 10 μm on either side of the movable beam. This is to account for the fringing effects of the electrostatic field that is generated in the medium between the two electrodes. We solve the boundary integral equations along with the equations describing the mechanical displacement in a coupled manner to obtain the final deformed configuration of the actuator under a static applied voltage. Suitable postprocessing can be applied to the mechanical displacement and electrostatic potential fields to obtain the output quantities of interest for which we are interested in performing uncertainty analysis. From Eq. (12)–(18), we can readily see that the coupled nature of the above multiphysics model would cause uncertainties in geometrical dimensions as well as material properties to be propagated through the model and ultimately result in variations in the displacement of the actuator. In Section 4.2, we show how the deterministic solver described above can be used in the UQ framework to predict the uncertainty in the actuator behavior.

### 4.2 Identification of Stochastic Model

We examine the effect of spatial uncertainties on the electrostatic microactuator described above. In this work, we restrict our focus to uncertainties in geometrical dimensions rather than in material properties. We examine a test case where the top surface of the ground plate has a rough profile and can be considered as a spatially varying uncertainty that modulates the interelectrode gap. Because the focus of this paper is the modeling of spatial uncertainties, we do not worry about the physical origin of these fluctuations. Instead we assume that we are given profilometric data of the interelectrode gap at discrete points along the length of the device and that the data are aggregated across different devices. Possible sources of uncertainty in the microfabrication process are spatial variations in deposition/etching of materials, nonuniformities in the thickness of photoresist films that are used as sacrificial layers in a surface micromachining workflow, etc. For the purpose of this work, we assume that the spatial variations are not significant in the direction perpendicular to the plane of movement of the actuator (shown in Fig. 11). This is a reasonable assumption if the thickness of the device in that direction is small compared to the length of the device.

Our first task is to generate data sets from a known random process and then estimate the stochastic variation from the data. The estimated process can then be propagated through the physical model along with the actual process in order to demonstrate the effectiveness of estimating spatial uncertainties in this manner. Following the same procedure described in previous sections, we generate data from a known random process that is defined in the domain $[-10, 110]$ μm. We pick a linear mean function, $M(X) = (0.05 + 0.005X)$ μm, and a Matérn covariance function with the parameters $\phi = 0.1$ μm, $\nu = 2$, and $\theta = 20$ μm. To simplify notation, we introduce a normalized spatial coordinate $X_n = (X + 10)/120$, such that $X_n \in [0, 1]$, and redefine the mean function in terms of $X_n$ as $M(X_n) = 0.6X_n$. It is easily seen that the spatial roughness profile that we have chosen causes the top surface of the ground plate to tilt upward, reducing the gap at the right end of the cantilever to ∼70% of its original value of 2 μm on average. The choice of the mean function profile is arbitrary, but the parameters that contribute to the spatial roughness profile are based on physically measured roughness profiles of photoresist films [33].

Nonstationarity is introduced using a virtual displacement function, and we choose two cases to demonstrate two different forms of nonstationarity. We denote $u(X_n) = X_n(1 - X_n)(2 - X_n)$ as Case I. This corresponds to a virtual displacement that is directed toward the right side or the free end of the actuator, because it is positive in the given domain. Case II is the opposite with $u(X_n) = -X_n(1 - X_n^2)$, which corresponds to a displacement that is directed toward the left side or the anchored end. In both cases, the form of the displacement function has been chosen such that it is zero at $X_n = 0, 1$, which are the left and right boundaries of the domain. Figures 12 and 13 show a contour

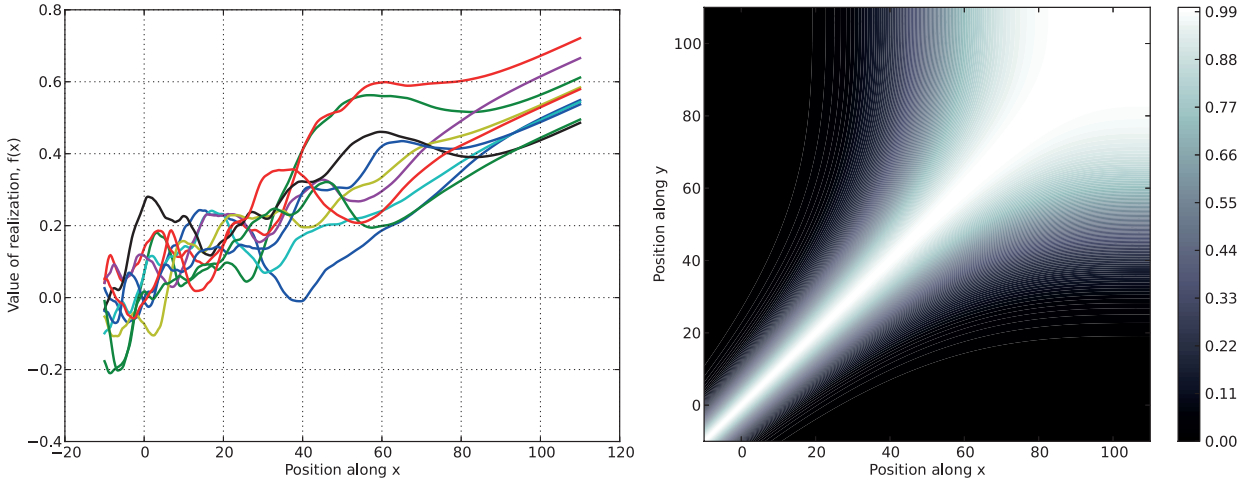


(a) Realizations of the actual stochastic process (b) Covariance function

**FIG. 12:** Actual nonstationary stochastic process corresponding to Case I illustrated by (a) sampled realizations and (b) contour plot of the covariance between points in the domain.

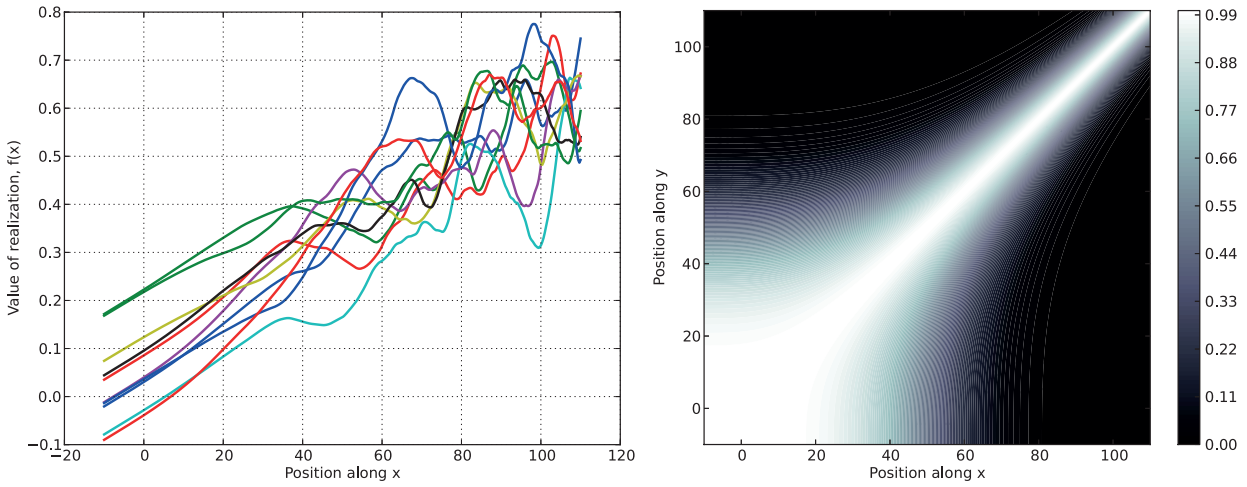


(a) Realizations of the actual stochastic process (b) Covariance function

**FIG. 13:** Actual nonstationary stochastic process corresponding to Case I illustrated by (a) sampled realizations and (b) contour plot of the covariance between points in the domain.

plot of the covariance function and a few realizations sampled from the stochastic processes corresponding to Cases I and II, respectively. The trends followed by the random functions obey the behavior seen in Section 3, where regions of compressive virtual strain are comparatively smoother than regions in tension.

Using the data sets generated for Cases I and II, we estimate the corresponding stochastic processes. We use a nonstationary formulation that is very similar to Eq. (6), except that we use the corrected form of the displacement function, having shown that it is equivalent to the regular polynomial form in Section 4.1. The final formulation is given by

$$\begin{aligned} f|M,C &\sim GP\left(M,C\right), \\ M : X_n, a, b, c &\mapsto aX_n^2 + bX_n + c, \\ X_n : X &\mapsto (X+10)/120 \\ C : x, x', \nu, \phi, \theta &\mapsto \text{Matérn}\left(x, x', \nu, \phi, \theta\right), \\ x : X_n, u &\mapsto -10 + 120(X_n + u(X_n)) \\ u : X_n, a_u, b_u &\mapsto a_u X_n^3 + b_u X_n^2 - (a_u + b_u)X_n, \\ \boldsymbol{d}|M,C &\sim \mathcal{N}\left(M(\boldsymbol{X}), C(x(\boldsymbol{X}), x(\boldsymbol{X}))\right), \end{aligned} \tag{19}$$

Expressing the formulation in terms of the normalized spatial coordinate helps to define the problem in terms of unknown parameters that are scale independent. This makes the formulation very flexible for modeling uncertainties defined over spatial domains of any scale. We can now assign the following prior PDFs for the unknown parameters, which are very similar to the ones that we have been using thus far,

$$\begin{aligned} a, b, c &\sim \text{Uniform}\left[-1, 1\right], \\ \nu &\sim \text{Exponential}\left(10\right), \\ \phi &\sim \text{Exponential}\left(20\right) \\ \theta &\sim \text{Exponential}\left(0.1\right) \\ a_u, b_u &\sim \text{Uniform}\left[-5, 5\right]. \end{aligned} \tag{20}$$

We generate 250 random realizations from the original stochastic process and sample each one at 41 uniformly spaced points in the domain to generate the simulated profilometric data for the random ground plate. Bayesian estimation is performed using the MCMC method with a burn-in of 30,000 samples and a thinning factor of 10. The resulting posterior distribution of the parameters can be used to obtain the estimated stochastic process that incorporates a nonstationary covariance model. We also estimate a different stochastic process that has exactly the same formulation as that mentioned in Eq. (19), but the virtual displacement function, $u(X_n)$, set to zero. This corresponds to a stationary covariance model, and we compare the resulting stochastic process to the one that uses a nonstationary model. Realizations drawn from both these processes are shown in Figs. 14 and 15 for Cases I and II, respectively. Comparing to Figs. 12 and 13, we see that the nonstationary model shows a good qualitative match with the actual random process. With the stationary model, although the mean trend is similar, the spatial variation of roughness is not captured at all, because this is a property of the nonstationarity in the covariance function.

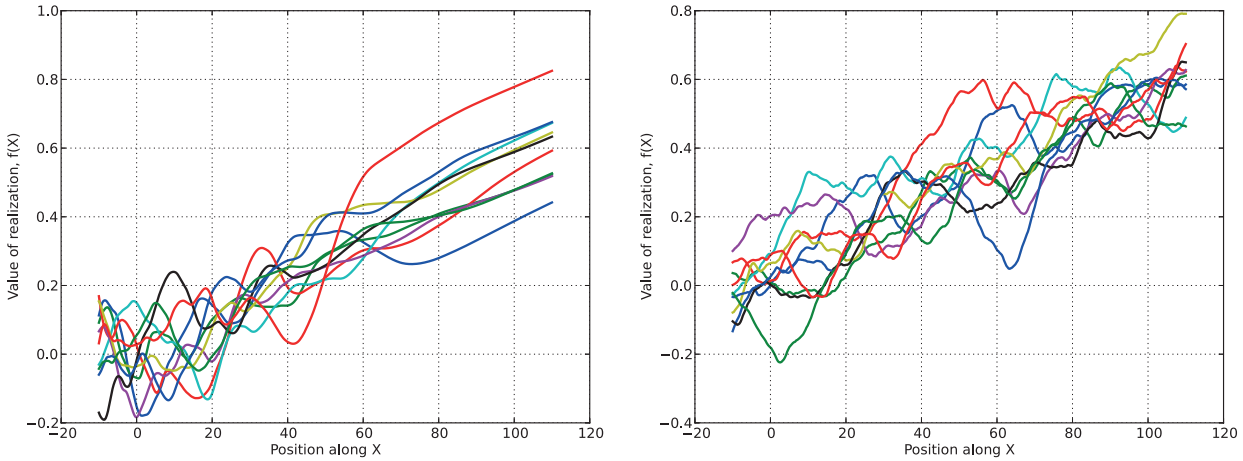


(a) Nonstationary model (b) Stationary model

**FIG. 14:** Realizations sampled from estimated stochastic process using (a) nonstationary and (b) stationary covariance function for data corresponding to Case I.

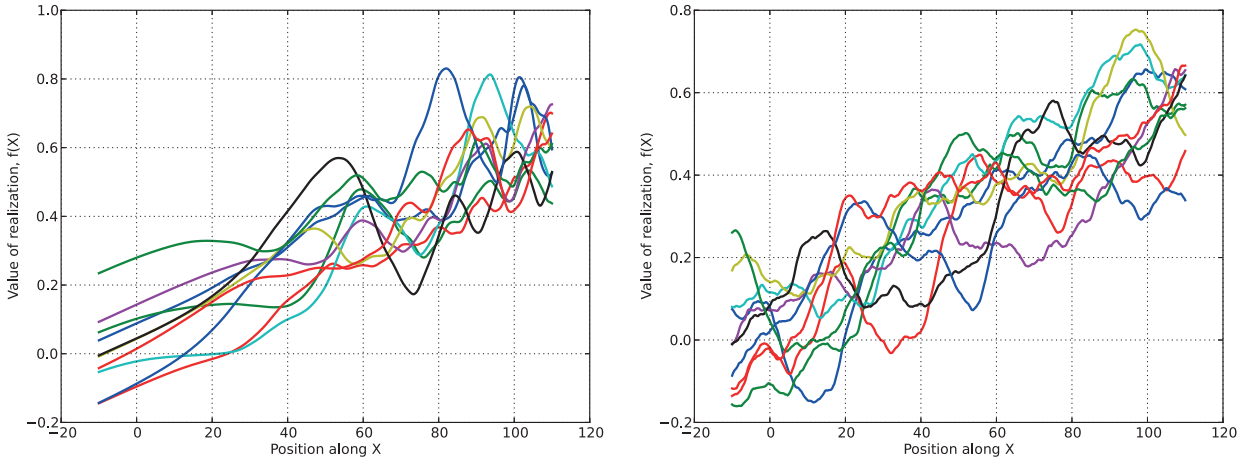


(a) Nonstationary model (b) Stationary model

**FIG. 15:** Realizations sampled from estimated stochastic process using (a) nonstationary and (b) stationary covariance function for data corresponding to Case II.

### 4.3 Electrostatic Analysis

We first perform a pure electrostatic analysis on the actuator in the presence of the spatial uncertainties. In this simulation, we do not consider the effect of electrostatic force and therefore assume that the top electrode does not move at all. We propagate the actual stochastic model as well as the estimated fields obtained using the nonstationary and stationary formulations. For each case, we modulate the top surface of the ground plate by a realization sampled from the stochastic process and then regenerate the mesh for the ground plate in order to perform finite element analysis. We solve Eq. (16) along with its boundary condition given by Eq. (18) and obtain the electrostatic potential along a plane lying mid-way between the two electrodes at a distance of 1 μm from the top electrode. These potential values are normalized by the maximum applied potential difference and plotted in Fig. 16 for both Cases I and II.

For the given actuator geometry, because we know that electrostatic potential varies fairly linearly within the gap between the electrodes, we expect that the spatial trend in the electrostatic potential will closely follow the roughness profile of the ground plate. This is confirmed by the trends seen in Fig. 16. This shows that the spatial uncertainty has been propagated into the electrostatic domain and the resulting transformation is quite linear. We see that in both cases, the nonstationary model reproduces the results corresponding to the actual stochastic process very well. The stationary model, on the other hand, is not able to capture any aspect of the spatial variation except for average behaviour.

### 4.4 Mechanical Displacement

We now include the effect of electrostatic force by performing a complete electromechanical analysis on the actuator to compute the mechanical displacement field. We solve for the downward displacement of the top electrode due to the electrostatic force and compute the variation of electrode tip displacement due to the effect of the spatial uncertainties. Here the spatial variation in the electrostatic potential will translate into the traction term and will result in a nonuniform electrostatic pressure being applied on the top electrode. Moreover, because the electrostatic force is

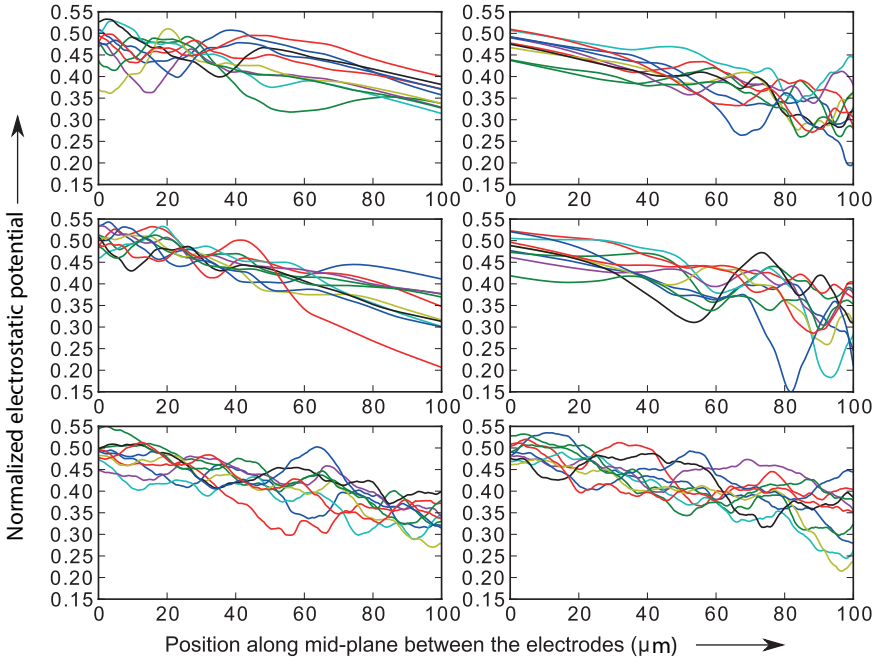


**FIG. 16:** Normalized electrostatic potential along the mid-plane for several realizations of the random field. The left column corresponds to Case I while the right column corresponds to Case II. The rows correspond to the results obtained using the actual stochastic process (top) and the estimated results using the nonstationary model (middle) and the stationary model (bottom).

inversely dependent on the local gap between two points on the top and bottom electrodes, as the actuator deforms, the electrostatic traction changes accordingly and exerts an additional nonlinear influence on the resulting displacement field.

We observe the effect of this nonlinear dependence in Fig. 17, where the device is actuated using a potential difference of 8 V and the PDF of tip displacement is plotted for the actual, nonstationary and stationary models for Cases I and II. If the tip displacement is linearly dependent on the input uncertainty, we would expect to see a symmetric variation about some nominal value. Instead we see that the tails of the distributions have been stretched more to the left, toward the region of greater displacement (more negative values). Comparing the PDFs for Cases I and II using the actual process (solid and dashed lines with circles), we see that the spread in tip displacement for Case I is almost three times the amount seen for Case II. To explain this difference, we look at the realizations and note that in Case I the realizations are relatively smoother on the right side of the domain, close to the tip of the actuator, whereas in Case II, the smoother regions are closer to the anchored end of the cantilever. In general, if the inter electrode gap fluctuates sharply about a mean value, then the positive and negative contributions tend to cancel out and the resulting electrostatic force is no different from the mean trend. However, if the spatial profile changes slowly, there is a greater degree of correlation between the values of electrostatic force at neighboring points and this results in a net increase or decrease in the local electrostatic force. When this increase or decrease occurs near the tip of the cantilever (as in Case I), its effect on the tip displacement is more pronounced than when it happens close to the anchored end of the cantilever (Case II). This is clearly seen in Fig. 17, where we note that the range of tip displacement increases almost three fold going from Cases II to I.

Between the three models, we again see a close match between the nonstationary model (solid and dashed lines with squares) and the actual one, whereas there is a significant discrepancy in the results predicted by the stationary model (solid and dashed lines with triangles). In fact, the stationary model is unable to even differentiate between Cases I and II, and ends up predicting a trend that is close to the average of the two. This shows the importance of using a nonstationary model to represent spatial uncertainties, because we clearly see that capturing the mean trend using a stationary covariance model is not sufficient to accurately reproduce the variation in tip displacement. Instead we need an inhomogeneous model that can correctly include spatial variations. This is crucial especially when the physical system has a nonlinear dependence on the input uncertainty, which causes the effect of nonstationarity to become amplified.

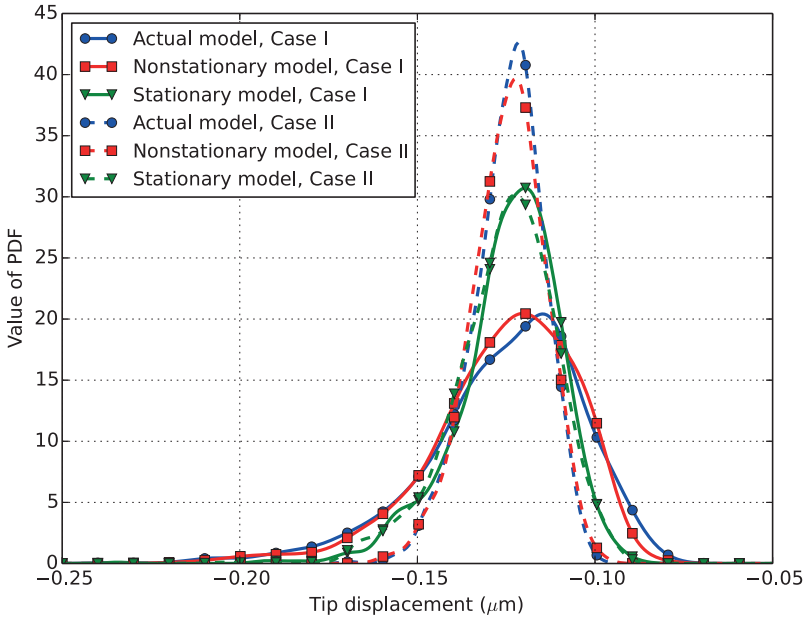


**FIG. 17:** Variation in tip displacement of the actuator under the effect of various stochastic models.

### 4.5 Pull-in Voltage

Electrostatic MEMS actuators are known to be subject to an instability phenomenon called pull-in. When the actuation voltage rises high enough, the mechanical restoring force in the deformable electrode is unable to resist the electrostatic force and the top electrode crashes onto the ground plate. The voltage at which this happens is known as the pull-in voltage and is a characteristic quantity for a given electrostatic actuator. It is also a quantity of interest in the design of electrostatic switches, where the pull-in phenomenon is used to make the device behave like a mechanical switch.

We perform a complete electromechanical analysis on the actuator by considering the effect of the electrostatic force. We use the bisection method to solve for the pull-in voltage for the case of the actual stochastic model as well as the estimated fields obtained using the nonstationary and stationary formulations. The results are shown in Fig. 18. For Case I, the pull-in voltage varies between 8.5 V and 16 V, while this range drops down by half when Case II is considered. With regard to the estimated models, we see a similar trend as that seen in the previous section. Again, the nonstationary model gives the best results, whereas the stationary model is unable to differentiate between Cases I and II. This shows the importance of using the correct stochastic model when including the effect of spatial uncertainties in electrostatic microactuators.

## 5. CONCLUSIONS

This paper presents a data-driven method of estimating stochastic models that describe spatial uncertainties in electrostatic microactuators. In order to quantify the effect of these uncertainties in MEMS, we develop a nonstationary formulation to handle heterogeneous random processes. The transformation function used to introduce nonstationarity is specified as an additive displacement that transforms the coordinate space to a deformed configuration in which the covariance between points can be represented by a stationary model. A Bayesian estimation involving the Markov Chain Monte Carlo (MCMC) method is used to estimate the parameters of the stochastic model from sets of data that are assumed to be independent and identically distributed. This approach is then used to model spatial uncertainties in microelectromechanical actuators, where the ground plate is assumed to have a spatially varying profile. The idea is to leverage existing spatial statistics modeling techniques to bring spatial uncertainties into the realm of uncertainty quantification, especially for micromechanical systems. This allows us to demonstrate the effect of these uncertainties on the displacement of the actuator as well as on other parameters, such as the pull-in voltage. By estimating the stochastic model using synthetic profilometric data, we demonstrate how experimental measurements of the ground plate surface roughness can be used to predict the variation in performance of these devices.

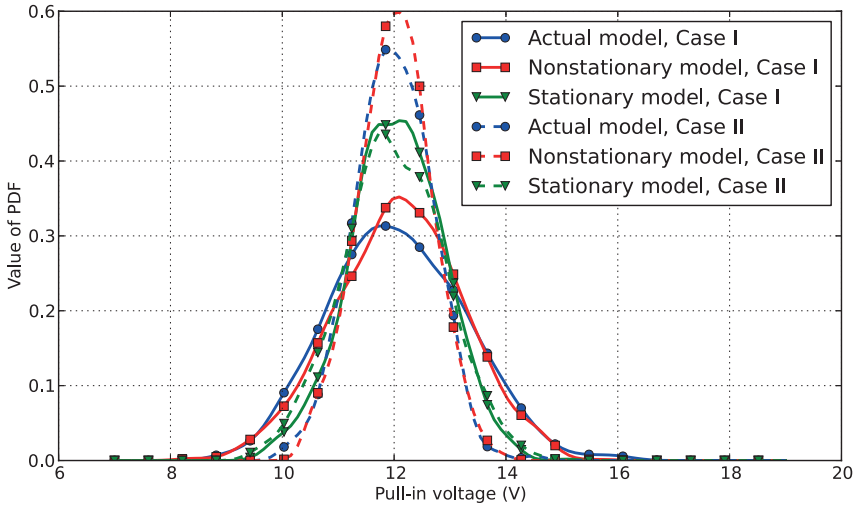


**FIG. 18:** Variation in pull-in voltage of the actuator under the effect of various stochastic models.

We show that nonstationarity is essential for accurate modeling of spatial uncertainties in electrostatic microactuators by presenting results that show the effect of nonstationary random processes on the electrical and mechanical behavior of microactuators. Although a stationary model can approximate the average trend to a reasonable extent, the nonlinearities in the physical model get amplified in the presence of nonstationary uncertainties. This difference is seen in the shape of the resulting PDF of any output quantity and most notably manifests itself by modifying the expected range of variation. We see that accurate modeling of the nonstationarity in the data is important when trying to predict the variation in the performance of these devices and hence emphasize the necessity for the inclusion of nonstationarity during stochastic modeling.

## ACKNOWLEDGMENTS

This work is supported by the National Science Foundation under Grant No. 1420882. The authors gratefully acknowledge the use of the parallel computing resource provided by the Computational Science and Engineering (CSE) Program at the University of Illinois. The CSE computing resource, provided as part of the Taub cluster, is devoted to high-performance computing in engineering and science.

## REFERENCES

1. Senturia, S., Aluru, N., and White, J., Simulating the behavior of MEMS devices: Computational methods and needs, *Comput. Sci. Eng.*, 4(1):30–43, 1997.
2. Aluru, N. and White, J., An efficient numerical technique for electromechanical simulation of complicated microelectromechanical structures, *Sens. Actuators A*, 58(1):1–11, 1997.
3. Li, G. and Aluru, N., Efficient mixed-domain analysis of electrostatic MEMS, *Comput.-Aided Des. Integr. Circ. Syst.*, 22(9):1228–1242, 2003.
4. Price, R. H., Wood, J. E., and Jacobsen, S. C., Modelling considerations for electrostatic forces in electrostatic microactuators, *Sens. Actuators*, 20(1-2):107–114, 1989.
5. Agarwal, N. and Aluru, N., A stochastic Lagrangian approach for geometrical uncertainties in electrostatics, *J. Comput. Phys.*, 226(1):156–179, 2007.
6. Agarwal, N. and Aluru, N. R., Stochastic analysis of electrostatic MEMS subjected to parameter variations, *J. Microelectromech. Syst.*, 18(6):1454–1468, 2009.
7. Alwan, A. and Aluru, N. R., Uncertainty quantification of MEMS using a data-dependent adaptive stochastic collocation method, *Compu. Methods Appl. Mech. Eng.*, 200(45):3169–3182, 2011.
8. Patrikar, R. M., Modeling and simulation of surface roughness, *Appl. Surf. Sci.*, 228(1):213–220, 2004.
9. Lepage, S., Stochastic finite element method for the modeling of thermoelastic damping in micro-resonators, PhD thesis, University of Liège, 2006.
10. Williams, C. K. and Rasmussen, C. E., *Gaussian Processes for Machine Learning*, MIT Press, Cambridge, MA, 2006.
11. Kennedy, M. C. and O'Hagan, A., Bayesian calibration of computer models, *J. R. Stat. Soc. Series B*, 63(3):425–464, 2001.
12. Cressie, N. A., *Statistics for Spatial Data*, rev. ed., Vol. 928, Wiley, Haboken, NJ, 1993.
13. Williams, C. K. I. and Rasmussen, C. E., Gaussian processes for regression, In *Advances in Neural Information Processing Systems 8*, MIT press, Cambridge, MA, pp. 514–520, 1996.
14. Besag, J., Spatial interaction and the statistical analysis of lattice systems, *J. R. Stat. Soc. Series B*, 36(2):192–236, 1974.
15. Bjørnstad, O. and Falck, W., Nonparametric spatial covariance functions: estimation and testing, *Env. Ecol. Stat.*, 8(1):53–70, 2001.
16. Zhu, Z. and Liu, Y., Estimating spatial covariance using penalised likelihood with weighted $L_1$ penalty, *J. Nonparametric Stat.*, 21(7):925–942, 2009.
17. Balram, N. and Moura, J., Noncausal Gauss Markov random fields: parameter structure and estimation, *IEEE Trans.*, 39(4):1333–1355, 1993.
18. Ferreira, M., Higdon, D., Lee, H., and West, M., Multi-scale random field models, ISDS Discussion Paper No. 05, 2005.

19. Sayles, R. S. and Thomas, T. R., Surface topography as a nonstationary random process, *Nature*, 271:431–434, 1978.
20. Sampson, P. D. and Guttorp, P., Nonparametric estimation of nonstationary spatial covariance structure, *J. Am. Stat. Assoc.*, 87(417):108–119, 1992.
21. Perrin, O. and Meiring, W., Identifiability for non-stationary spatial structure, *J. Appl. Probab.*, 36(4):1244–1250, 1999.
22. Perrin, O. and Senoussi, R., Reducing non-stationary random fields to stationarity and isotropy using a space deformation, *Stat. Probab. Lett.*, 48(1):23–32, 2000.
23. Damian, D., Sampson, P. D., and Guttorp, P., Bayesian estimation of semi-parametric non-stationary spatial covariance structures, *Env.*, 12(2):161–178, 2001.
24. Gamerman, D. and Lopes, H. F., *Markov Chain Monte Carlo: Stochastic Simulation for Bayesian Inference*, Vol. 68, Chapman & Hall/CRC, Boca Raton, 2006.
25. Patil, A., Huard, D., and Fonnesbeck, C. J., PyMC: Bayesian stochastic modelling in Python, *J. Stat. Softw.*, 35(4):1–81, 2010.
26. Toni, T. and Stumpf, M. P. H., Simulation-based model selection for dynamical systems in systems and population biology, *Bioinformatics*, 26(1):104–110, 2010.
27. Jeffreys, H., *The Theory of Probability*, Oxford University Press, London, 1998.
28. Chandrasekharaiah, D. S. and Debnath, L., *Continuum Mechanics*, Academic Press, New York, 1994.
29. Parkus, H., *Thermoelasticity*, Blaisdell Publishing, New York, 1968.
30. Jaswon, M. and Symm, G., *Integral Equation Methods in Potential Theory and Elastostatics*, Academic Press, New York, 1977.
31. Shi, F., Ramesh, P., and Mukherjee, S., On the application of 2D potential theory to electrostatic simulation, *Commun. Numer. Methods Eng.*, 11(8):691–701, 1995.
32. Alwan, A. and Aluru, N., Analysis of hybrid electrothermomechanical microactuators with integrated electrothermal and electrostatic actuation, *J. Microelectromech. Syst.*, 18(5):1126–1136, 2009.
33. Poutous, M. K., Hosseinimakarem, Z., and Johnson, E. G., Photoresist surface roughness characterization in additive lithography processes for fabrication of phase-only optical vortices, *J. Micro/Nanolithog. MEMS MOEMS*, 11(4):043009, 2012.